Optimizing future imaging survey of galaxies to confront dark energy and modified gravity models

Kazuhiro Yamamoto

Graduate School of Science, Hiroshima University, Higashi-Hiroshima, 735-8526, Japan

David Parkinson

Astronomy Centre, University of Sussex, Brighton BN1 9QH, United Kingdom

Takashi Hamana

National Astronomical Observatory of Japan, 2-21-1 Osawa, Mitaka, Tokyo, 181-8588, Japan

Robert C. Nichol

ICG, University of Portsmouth, Portsmouth, PO1 2EG, United Kingdom

Yasushi Suto

Department of Physics and Research Center for the Early Universe, The University of Tokyo, Tokyo 113-0033, Japan

We consider the extent to which future imaging surveys of galaxies can distinguish between dark energy and modified gravity models for the origin of the cosmic acceleration. Dynamical dark energy models may have similar expansion rates as models of modified gravity, yet predict different growth of structure histories. We parametrize the cosmic expansion by the two parameters, w_0 and w_a, and the linear growth rate of density fluctuations by Linder's γ, independently. Dark energy models generically predict $\gamma \approx 0.55$, while the Dvali-Gabadadze-Porrati (DGP) model $\gamma \approx 0.68$. To determine if future imaging surveys can constrain γ within 20% (or $\Delta\gamma < 0.1$), we perform the Fisher matrix analysis for a weak-lensing survey such as the ongoing Hyper Suprime-Cam (HSC) project. Under the condition that the total observation time is fixed, we compute the figure of merit (FoM) as a function of the exposure time $t_{\rm exp}$. We find that the tomography technique effectively improves the FoM, which has a broad peak around $t_{\rm exp} \simeq$ several ~ 10 min; a shallow and wide survey is preferred to constrain the γ parameter. While $\Delta\gamma < 0.1$ cannot be achieved by the HSC weak-lensing survey alone, one can improve the constraints by combining with a follow-up spectroscopic survey like Wide-field Fiber-fed Multi-Object Spectrograph (WFMOS) and/or future cosmic microwave background (CMB) observations.

I. INTRODUCTION

The existence of the mysterious cosmic acceleration is usually ascribed to the presence of an extra component of the Universe with a negative pressure, known as dark energy. However, modification of the law of gravity remains as another interesting and equally valid possibility. One of the most elaborated examples is the Dvali-Gabadadze-Porrati (DGP) cosmological model that incorporates the self-acceleration mechanism [1,2] without dark energy. A fundamental question in this context is whether it is possible to distinguish between the modified gravity and dark energy models that have an (almost) identical cosmic expansion history [3,4]. The answer to the question is inevitably dependent on the specific model of dark energy or modified gravity [5]. Thus we focus on the DGP model, and consider if it has any observational signature that can be distinguished from dark energy models with future galactic surveys. While it is pointed out that the DGP model has some theoretical inconsistency at a fundamental level [6–8], it is still useful as an empirical prototype of

modified gravity models, and its observational consequences are discussed [3,9–11].

The important key is the growth rate of cosmological density perturbations, which should be different in the two models even if they have an identical cosmic expansion history. The weak-lensing power spectrum can be sensitive to the growth rate, while the uncertainty of the clustering bias will be the bottleneck that makes the galaxy power spectrum insensitive to the growth rate.

Currently several imaging and spectroscopic surveys of galaxies are planned to unveil the origin of cosmic acceleration via weak-lensing and baryon acoustic oscillation methods. The Hyper Suprime-Cam (HSC) project is a fully funded imaging survey at the Subaru telescope, which is expected to commission in 2011. An associated spectroscopic survey possibility, Wide-field Fiber-fed Multi-Object Spectrograph (WFMOS) project, is under serious discussion between Subaru and Gemini observatories (see e.g. [12,13] and references therein for other projects).

In the present paper, we consider the extent to which future imaging and spectroscopic surveys of galaxies can

distinguish between the DGP and dark energy models. More specifically, we empirically characterize the growth rate of density fluctuations adopting Linder's γ parameter. By optimizing imaging surveys and the combination with redshift survey following the previous literature [14,15], we consider how we can constrain the value of γ from HSC weak-lensing survey and/or WFMOS baryon acoustic oscillation (BAO) survey.

The present paper is organized as follows: In Sec. II, we explain our theoretical modeling: the parametrization of the background expansion and the modified gravity, the Fisher matrix analysis of the weak-lensing power spectrum, and the modeling of the galaxy sample. A demonstration with the DGP model and dark energy model is also presented. In Sec. III, our result of the Fisher matrix analysis is presented. Section IV is devoted to summary and conclusions. Throughout the paper, we use the units in which the speed of light is unity.

II. THEORETICAL MODELING

In this analysis we consider a spatially flat universe for simplicity, consisting of baryons, cold dark matter, and dark energy. We ignore the dark energy clustering, and assume that the spatial fluctuations entirely originate from the matter component (i.e., baryons and dark matter). We further model that the cosmic expansion history *effectively* follows the Universe with the matter density parameter Ω_m and the dark energy parameter $1 - \Omega_m$:

$$H(a)^2 = H_0^2[\Omega_m a^{-3} + (1 - \Omega_m)a^{-3(1+w_0+w_a)}e^{3w_a(a-1)}],$$
(2.1)

where $H_0 = 100h \text{ km s}^{-1} \text{ Mpc}^{-1}$ is the Hubble constant, a is the cosmic scale factor, and w_0 and w_a are constants parametrizing the equation of state of dark energy [16–18]:

$$p/\rho \equiv w(a) = w_0 + w_a(1 - a).$$
(2.2)

Note that we use Eq. (2.1) even in the DGP model that does not have dark energy at all by approximating its cosmic expansion law with the two parameters w_0 and w_a. In this case, they do not have any relations to dark energy in reality, but it is already shown that such an empirical description provides a reasonable approximation to the cosmic expansion in the DGP model. For definiteness, the expansion in the DGP has the *effective* equation of state (e.g., [19])

$$w(a) = -\frac{1}{1 + \Omega_m(a)},$$
(2.3)

where

$$\Omega_m(a) = \frac{H_0^2 \Omega_m a^{-3}}{H(a)^2}.$$
(2.4)

The cosmic expansion in the DGP model is well approximated by the dark energy model with *effective* equation of

state with $w_0 = -0.78$ and $w_a = 0.32$ as long as $\Omega_m \sim 0.27$. The parametrization gives the distance redshift relation within 0.5% out to the redshift 2 [19].

A. Linder's γ parameter

According to Refs. [19–21], the linear growth factor in the DGP and dark energy models is well approximately expressed by

$$D_1(a) = \exp\left[\int_0^a \frac{da'}{a'}(\Omega_m(a')^\gamma - 1) \right].$$
(2.5)

In this description, the constant parameter γ characterizes the gravity force model, i.e., the Poisson equation.

The dark energy models with the effective equation of state (2.2) within the general relativity are well approximated by

$$\gamma = 0.55 + 0.05[1 + w(z = 1)] \quad (w > -1), \quad (2.6)$$

$$\gamma = 0.55 + 0.02[1 + w(z = 1)] \quad (w < -1). \quad (2.7)$$

This formula reproduces the exact linear growth factor within 0.3% (0.5%) for $-1.2 < w < -0.8$ ($-1.5 < w < -0.5$). Therefore γ in dark energy models takes the value $\gamma = 0.54$–0.56 for $-1.2 < w < -0.8$ [19–21].

On the other hand, in the DGP model, the Poisson equation is modified in the linear regime. Then γ takes a different value from that of the dark energy model even if the background expansion is the same (i.e. if w_0 and w_a are same). Reference [21] found that in the DGP model $\gamma = 0.68$ is an excellent approximation for the evolution of the growth factor and that γ varies by only 2% into the past.

The point here is that a dark energy model mimicking the cosmic expansion history of the DGP model predicts a different linear growth rate by $\Delta\gamma \sim 0.1$. In what follows, therefore, we employ Eqs. (2.1), (2.2), (2.3), and (2.4) to describe the expansion history and the growth of density fluctuations, which empirically describe both the DGP and dark energy models, and ask if it is possible to achieve the accuracy of $\Delta\gamma \sim 0.1$ by optimizing future surveys of galaxies.

B. Weak-lensing power spectrum and Fisher matrix

The optimization of imaging surveys is based on the weak-lensing tomography method (see e.g., [22–25]). In this methodology, one divides the entire galaxy samples in several different redshift bins according to the weight factor $W_i(z(\chi))$ for the ith redshift bin:

$$W_i(z) = \frac{1}{\bar{N}_i} \int_{\max(z_i,z)}^{z_{i+1}} dz' \frac{dN(z')}{dz'}\left(1 - \frac{\chi(z)}{\chi(z')}\right),$$
(2.8)

where dN/dz denotes the differential number count of galaxies with respect to redshift per unit solid angle (see below for details), $\chi(z)$ is the radial comoving distance at z,

$$\chi(z) = \int_0^z \frac{dz'}{H(z)} = \frac{1}{H_0} \int_0^z \frac{dz'}{\sqrt{\Omega_m(1+z')^3 + (1-\Omega_m)(1+z')^{3(1+w_0+w_a)}e^{-3w_a z'/(1+z')}}}, \qquad (2.9)$$

and

$$\bar{N}_i = \int_{z_i}^{z_{i+1}} dz' \frac{dN(z')}{dz'} \qquad (2.10)$$

is the total number of galaxies in the ith redshift bin. While imaging surveys provide photometric redshifts alone from the multiband photometry, instead of spectroscopic redshifts, for galaxies, it is known that the lensing tomography works even with relatively crude redshift information.

Assuming that the anisotropic stress is negligible, the cosmic shear power spectrum is given as:

$$P_{(ij)}(l) = \int d\chi W_i(z(\chi)) W_j(z(\chi)) \left(\frac{3H_0^2 \Omega_m}{2a}\right)^2$$
$$\times P_{\text{mass}}^{\text{Nonlinear}}\left(k \to \frac{l}{\chi}, z(\chi)\right), \qquad (2.11)$$

where $P_{\text{mass}}^{\text{nonlinear}}(k, z)$ is the nonlinear mass power spectrum at the redshift z, k is the wave number of the three dimensional coordinates, l is the wave number of the two dimension corresponding to the angular coordinates, a is the scale factor normalized to unit at the redshift $z = 0$. We compute $P_{\text{mass}}^{\text{nonlinear}}(k, z)$ adopting the Peacock and Dodds formula [26].

The covariance matrix for $P_{(ij)}(l)$ is approximately given by

$$\text{Cov}[P_{(ij)}(l), P_{(mn)}(l')] = \frac{\delta_{ll'}}{(2l+1)\Delta l f_{\text{sky}}}[P_{(im)}^{\text{obs}}(l)P_{(jn)}^{\text{obs}}(l)$$
$$+ P_{(in)}^{\text{obs}}(l)P_{(jm)}^{\text{obs}}(l)]$$
$$\equiv \delta_{ll'}\text{Cov}_{(ij)(mn)}(l), \qquad (2.12)$$

where we define

$$P_{(ij)}^{\text{obs}}(l) = P_{(ij)}(l) + \delta_{ij}\frac{\sigma_\varepsilon^2}{\bar{N}_i}, \qquad (2.13)$$

f_{sky} is the fraction of the survey area, and σ_ε is the rms value of the intrinsic ellipticity of randomly oriented galaxies, for which we adopt $\sigma_\varepsilon = 0.4$ (see e.g., [22–24]).

Finally the Fisher matrix is estimated as

$$F_{\alpha\beta} = \sum_l \sum_{(ij)(mn)} \frac{\partial P_{(ij)}(l)}{\partial \theta^\alpha} \text{Cov}_{(ij)(mn)}^{-1}(l) \frac{\partial P_{(mn)}(l)}{\partial \theta^\beta}, \qquad (2.14)$$

where θ^α denote a set of parameters in the theoretical modeling. To be more specific, we consider 7 parameters, γ, w_0, w_a, Ω_m, σ_8 (the fluctuation amplitude at $8h^{-1}$ Mpc), h, and n_s (the primordial spectral index of matter power spectrum), assuming the other cosmological parameters are determined from independent cosmological data analysis.

We adopt the range of $10 \le l \le 10^4 \times (N_g/35/n_b)^{1/2}$ for the sum of l, where N_g is the number density of galaxy per unit solid angle (see next subsection). We define the 3-dimensional figure of merit (FoM) by the reciprocal of the volume of the error ellipsoid enclosing the 1 sigma confidence limit in the $\{\gamma, w_0, w_a\}$ space, marginalizing the Fisher matrix over the other parameters. Similarly, the 2-dimensional figure of merit is the reciprocal of the surface of the error ellipse enclosing the 1 sigma confidence limit in the $\{w_0, w_a\}$ plane with γ fixed.

C. Modeling galaxy sample

We assume the following form of the redshift distribution of the galaxy sample per unit solid angle

$$\frac{dN}{dz} = \frac{N_g \beta}{z_0^{\alpha+1}\Gamma((\alpha+1)/\beta)} z^\alpha \exp\left[-\left(\frac{z}{z_0}\right)^\beta\right], \qquad (2.15)$$

where α, β, and z_0 are the parameters, and $N_g = \int dz dN/dz$. The mean redshift may be determined by

$$z_m = \frac{1}{N_g} \int dz z \frac{dN}{dz} = \frac{z_0\Gamma((\alpha+2)/\beta)}{\Gamma((\alpha+1)/\beta)}. \qquad (2.16)$$

We assume that N_g and z_m is related to the exposure time t_{exp} as, following Ref. [14],

$$z_m = 0.9\left(\frac{t_{\text{exp}}}{30 \text{ min}}\right)^{0.067}, \qquad (2.17)$$

$$N_g = 35\left(\frac{t_{\text{exp}}}{30 \text{ min}}\right)^{0.44} \text{ arcmin}^{-2}. \qquad (2.18)$$

The mean redshift z_m changes from 0.72 to 1.1, and N_g does from 7.8 to 163, as the exposure time t_{exp} changes from 1 min to 10^3 min. In Ref. [14], $\alpha = 2$ and $\beta = 1.5$ are adopted. However, in the present paper, we adopt $\alpha = 0.5$ and $\beta = 3$.

In order to check the validity of our mock galaxy samples, we show in Fig. 1 the two cases of $\alpha = 0.5$ and $\beta = 3$ (dotted curve), and $\alpha = 2$ and $\beta = 1.5$ (dashed curve), for exposure times of $t_{\text{exp}} = 1, 5, 10, 30, 45$ minutes (from bottom to top, respectively). The solid curves show the real redshift histograms, for the corresponding i band magnitude limits, taken from the Canada-France-Hawaii telescope (CFHT) photometric redshift data of [27]. These photo-z's were calibrated using the VIMOS VLT deep survey (VVDS) spectroscopy and are reliable to $i \simeq 25$ which is sufficient for this study (see [27]). The relationship between magnitude limit and exposure time was scaled from the published Subaru Suprime-Cam data of [28]. These data are shown in Table I for the i, g, r, z
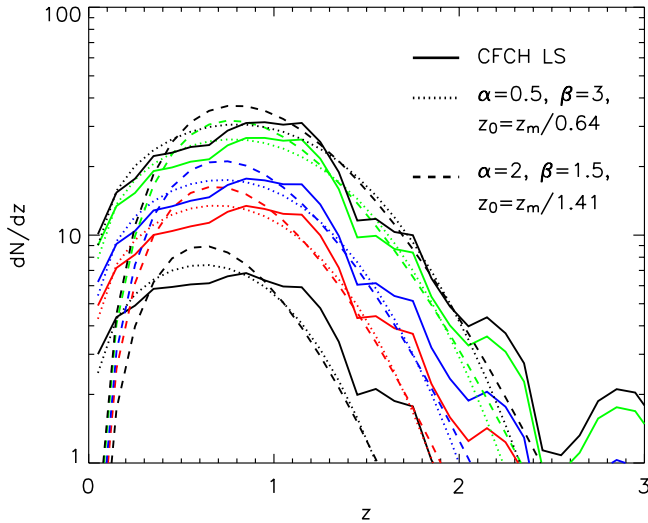
FIG. 1 (color online). dN/dz as a function of the exposure time, $\alpha = 2$, $\beta = 1.5$ with $z_0 = z_m/1.41$ (dashed curve), and $\alpha = 0.5$, $\beta = 3$ with $z_0 = z_m/0.64$ (dotted curve), respectively, for the fitting function of the form (2.15), for the exposure time $t_{exp} = 1, 5, 10, 30, 45$ minutes from bottom to top. The solid curve shows the corresponding CFHT LS photo-z i band data.

passbands. Denoting the exposure time for the i band by t_{exp}, the exposure time for the g band is about $t_{exp_g} = 3 \times t_{exp}$. Similarly, $t_{exp_r} = 1.2 \times t_{exp}$ for the r band, and $t_{exp_z} = 0.3 \times t_{exp}$ for the z band, respectively.

The total survey area can be expressed as

$$\text{area} = \pi \left(\frac{\text{field of view}}{2} \right)^2 \frac{T_{\text{total}}}{1.1 \times \sum_j t_{exp_j} + t_{op}}, \quad (2.19)$$

where we assume that the field of view of 1.5 °, the total observation time T_{total} is fixed as 800 hours, and the overhead time is modeled by a constant, $t_{op} = 5$ min, plus a fraction (10%) of the exposure time $\sum_j t_{exp_j}$ for one field of view.

We consider the cases the tomography is used, which we denote by $n_b = 2$, $n_b = 3$, and $n_b = 4$. Here n_b denotes the number of the redshift bin. In the case $n_b = 2$, the sample is divided into the two subsamples in the range $0.05 < z < z_m$ and $z_m < z < 2.5$, while in the case $n_b = 3$, we consider the three subsamples $0.05 < z < 3z_m/4$, $3z_m/4 < z < 5z_m/4$, and $5z_m/4 < z < 2.5$. In the case

TABLE I. Exposure time for the bands, i, g, r, z.

$i_{AB \ limit}$	$i(S/N = 10)$	$g(S/N = 5)$	$r(S/N = 5)$	$z(S/N = 5)$
22.97	1 min	3 min	1.1 min	0.3 min
23.84	5 min	15 min	7 min	1.4 min
24.22	10 min	30 min	12 min	3.5 min
24.81	30 min	90 min	34 min	8.1 min
25.04	45 min	130 min	50 min	13 min

$n_b = 4$, we consider the four subsamples $0.05 < z < 0.6 \times z_m$, $0.6 \times z_m < z < z_m$, $z_m < z < 1.4 \times z_m$, and $1.4 \times z_m < z < 2.5$ (see also Table II). We also consider the case the tomography is not used, which we denote by $n_b = 1$, for which we do not take into account how to obtain dN/dz, instead assuming that dN/dz is obtained by some method.

We assume that the subsample of $n_b = 2$ is constructed by the two band, r and i, observation, given that the strategy proposed in [29] is successful. The cases $n_b = 3$ and $n_b = 4$ are constructed by the 4 band g, i, r, z, observation, assuming that the conventional photo-z is successful. The case $n_b = 1$ is based on the i band observation. We assume that 90% galaxies of i band measurements dN/dz can be used as the subsample, in the case $n_b = 2, 3, 4$.

We use t_{exp} to represent the i band exposure time for one field of view, then we assume $\sum_j t_{exp_j} = 5.5 \times t_{exp}$ for the cases $n_b = 3, 4$, $\sum_j t_{exp_j} = 2.2 \times t_{exp}$ for the case $n_b = 2$, and $\sum_j t_{exp_j} = t_{exp}$ for the case $n_b = 1$, respectively.

Figure 2 shows the resultant total survey area, and the total number of galaxies as a function of the i band exposure time t_{exp}, for the cases, $n_b = 1, 2, 3$, and 4.

D. DGP model

Here we demonstrate the weak lens power spectrum of the dark energy model and the DGP model with the same cosmic expansion. The linear perturbation theory in the DGP model has been extensively worked out by [11]. While more recently Koyama and Silva studied nonlinear evolution of density fluctuations in the DGP model [30], the nonlinear nature of the gravity in the DGP model is still an unsolved problem. Therefore we adopt an empirical modeling of the nonlinear growth combining the
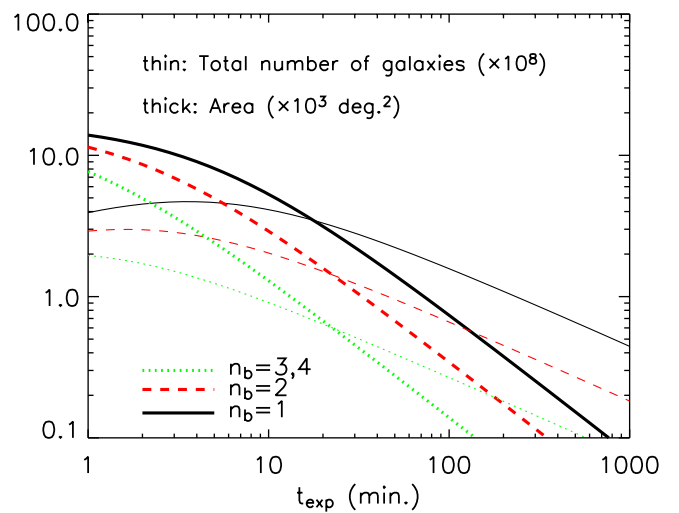

FIG. 2 (color online). The total survey area (thick line), and the total number of the galaxies (thin line) as a function of the i band exposure time t_{exp}, for the case $n_b = 1, 2, 3$, and 4.

TABLE II.   Assumption on the subsample and measurement.

Subsample	$n_b = 1$	$n_b = 2$	$n_b = 3$	$n_b = 4$
Choice of band	i	i, r	g, r, i, z	g, r, i, z
$\sum_j t_{\exp_j}$	$t_{\exp}$	$2.2 \times t_{\exp}$	$5.5 \times t_{\exp}$	$5.5 \times t_{\exp}$
Redshift bins	$0.05 < z < 2.5$	$0.05 < z < z_m$	$0.05 < z < 3z_m/4$	$0.05 < z < 0.6 \times z_m$
		$z_m < z < 2.5$	$3z_m/4 < z < 5z_m/4$	$0.6 \times z_m < z < z_m$
			$5z_m/4 < z < 2.5$	$z_m < z < 1.4 \times z_m$
				$1.4 \times z_m < z < 2.5$

Peacock-Dodds nonlinear fitting formula [26] and the linear growth rate in the DGP model [11]. As a result, our predictions below may be inaccurate on nonlinear scales, but our main conclusions concerning the optimization strategy would be unlikely to be sensitive to this approximation.

Figure 3 shows the weak shear power spectrum of the spatially flat DGP model and the dark energy model with the same background expansion. The cosmological parameters of both of the models are the same ($\Omega_m = 0.27$, $\Omega_b = 0.044$, $h = 0.72$, $\sigma_8 = 0.8$, and the spectral index $n_s = 0.95$). To realize the same cosmic expansion history, the *effective* equation of state parameter of the dark energy is chosen as $w(z) = -0.78 + 0.32z/(1 + z)$, as mentioned in Sec. II A. A similar computation has been already considered by [31], but our present work differs in that we use the Peacock and Dodds formula and that we assume a rather shallow sample of galaxies. Because the Poisson equation of the DGP model is modified, then the difference
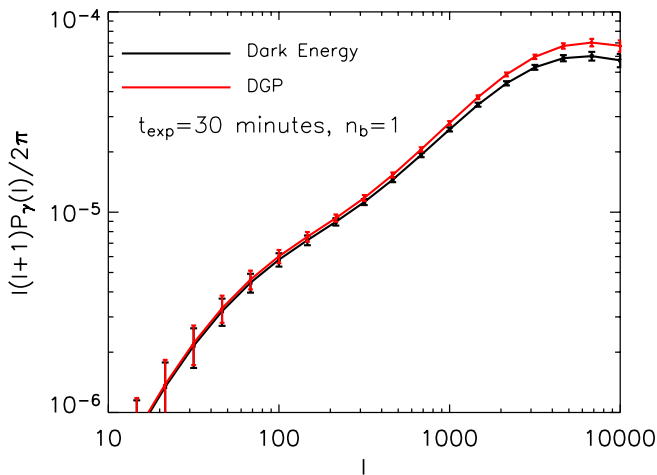

FIG. 3 (color online).   The dark curve is the weak-lensing power spectrum of the dark energy model with the cosmological parameter, $\Omega_m = 0.27$, $\Omega_b = 0.044$, $h = 0.72$, $\sigma_8 = 0.8$, $n_s = 0.95$, and the equation of state parameter of the dark energy $w_0 = -0.78$, $w_a = 0.32$, while the bright curve is the flat DGP model of the same cosmological parameters. Here we assume the HSC like survey with $t_{\exp} = 30$ min of the case $n_b = 1$ (see Sec. II for details).

comes from the growth rate. In this figure we assume 30 minutes exposure time of $n_b = 1$. The theoretical curves and the error bars depend on the survey sample, but we might expect that the two curves could be distinguished. In the next section, we examine the capability of the differentiation.

III. RESULTS

In this section, we present our optimization analyses for the HSC weak-lensing survey. Specifically, we fix the total observation time of the HSC survey, $T_{\rm tot}$ as 800 hours, and adopt a model of the background galaxy sample described in Sec. II C for the HSC survey; in particular, the mean redshift of galaxies z_m and their surface number density N_g are given by Eqs. (2.17) and (2.18) as a function of the exposure time $t_{\exp}$. In this section, we also present results in combination with a spectroscopic survey, the WFMOS BAO survey, which will be limited by a total observation time (see [15] for discussion of the optimization under this condition). Note that we also assume that the WFMOS survey is limited by the total survey area of the HSC imaging survey. Namely, the survey area of the WFMOS survey must be less than or equal to that of the HSC survey, as the HSC survey is acting as a photometric source catalogue for the WFMOS spectroscopic survey. So, for the WFMOS survey, we fix the same survey area as the HSC imaging survey Eq. (2.19), and the redshift range of galaxies $0.8 \leq z \leq 1.4$ with the number density $\bar{n} = 4 \times 10^{-4} h^3$ Mpc^{-3} [15], which is a set of optimized survey parameters for the spectroscopic survey.

Figure 4 shows the FoM of the 3-dimension (3D) of $\{\gamma, w_0, w_a\}$, as a function of the exposure time, $t_{\exp}$. The 3D FoM, the reciprocal of the volume of the 1σ error ellipsoid in the $\{\gamma, w_0, w_a\}$ space, is computed by marginalizing the Fisher matrix of the 7 parameters over Ω_m, σ_8, h, and n_s, with a fixed value for the baryon density, $\Omega_b = 0.044$.

The lensing tomography method with $n_b = 2$ significantly improves the 3D FoM, and continues to do so with increasing n_b for $t_{\exp} \lesssim 10$ min. The peak of the FoM systematically shifts to the shorter exposure time with larger n_b, while the peak profile is fairly broad. With increasing n_b, more information of redshift evolution of structure can be obtained. Similarly, as $t_{\exp}$ increases, more
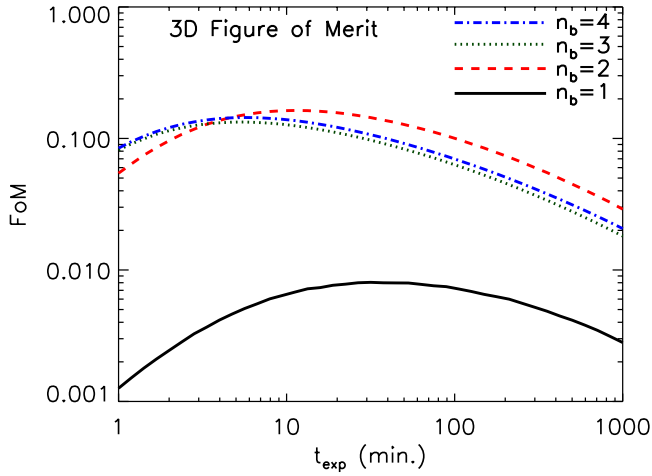
FIG. 4 (color online).   Three-dimensional FoM in $\{\gamma, w_0, w_a\}$ as a function of the i band exposure time, which is obtained from the Fisher matrix of the 7 parameters γ, w_0, w_a, Ω_m, σ_8, h, and n_s, Here the target parameter is $\gamma = 0.55$, $w_0 = -1$, $w_a = 0$, $\Omega_m = 0.27$, $\sigma_8 = 0.8$, $h = 0.72$, $n_s = 0.95$. The other parameter, $\Omega_b = 0.044$ is fixed.

FIG. 6 (color online).   1 sigma error in measuring γ as a function of the exposure time, obtained by marginalizing the Fisher matrix of the 7 parameters γ, w_0, w_a, Ω_m, σ_8, h, and n_s, over the parameters other than γ. The target parameters are the same as those of Fig. 4.

information of smaller structure can be obtained. However, these are offset by a decrease in total survey area. Namely, observation of more bands and longer exposures consume observation time, and the total survey area becomes smaller. This decreases the FoM.

For comparison, we plot in Fig. 5 the 2D FoM, the reciprocal of the area of the 1σ error ellipse in the $\{w_0, w_a\}$ plane, evaluated by marginalizing the Fisher matrix of the 6 parameters (w_0, w_a, Ω_m, σ_8, h, and n_s) with $\Omega_b = 0.044$ and $\gamma = 0.55$ fixed. One can find the similar
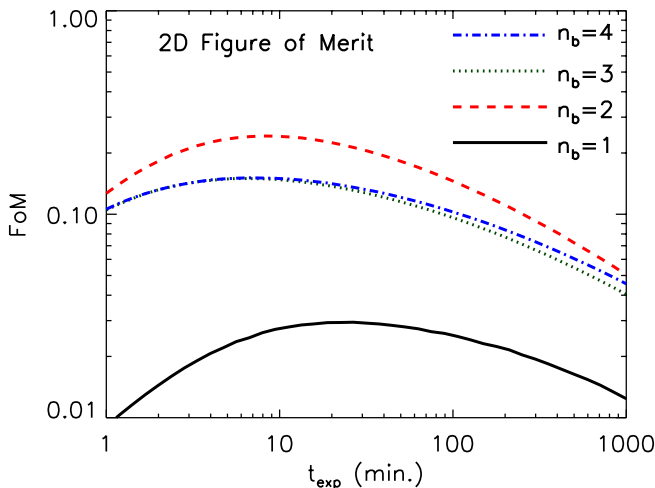

FIG. 5 (color online).   Two-dimensional FoM in $\{w_0, w_a\}$ from the Fisher matrix of the 6 parameters w_0, w_a, Ω_m, σ_8, h. Here the fiducial model is ΛCDM, with $w_0 = -1$, $w_a = 0$, $\Omega_m = 0.27$, $\sigma_8 = 0.8$, $h = 0.72$, $n_s = 0.95$. The other parameters, $\gamma = 0.55$ and $\Omega_b = 0.044$ are fixed.
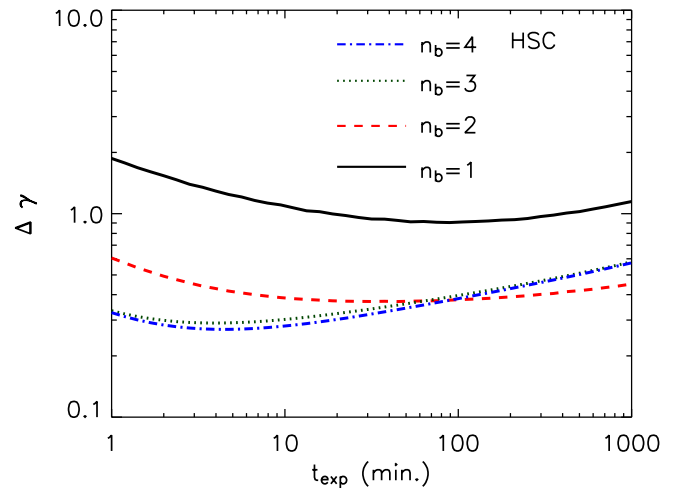
features as those of the 3D FoM. This figure suggests the three redshift bin is enough to constrain w_0 and w_a and that the peak of FoM is located around $t_{\rm exp} \approx 10$ min, and the peak profile is very broad. The FoM of the case $n_b = 2$ is larger than that of $n_b = 3, 4$. This indicates that the observation of the larger survey area with a small number of bands ($n_b = 2$) can be useful for the dark energy constraints, though an accurate-photo-z strategy is required.

Figure 6 shows the 1σ error on γ as a function of $t_{\rm exp}$, which is estimated by marginalizing the Fisher matrix of the 7 parameters, γ, w_0, w_a, Ω_m, σ_8, h, and n_s, over the parameters other than γ. The curve shows the error from the weak-lensing power spectrum adopting a proposed survey with HSC; $\Delta\gamma \approx 0.3(1)$ can be achieved with (without) tomography. The result indicates that the weak-lensing survey alone cannot reach the accuracy of $\Delta\gamma = 0.1$ that is required to distinguish between the DGP and dark energy models.

The uncertainty in γ can be significantly (more than a factor of 3) reduced by combining the baryon oscillation features from the WFMOS survey (Fig. 7). In modeling the galaxy power spectrum of the redshift survey, we simply considered the linear theory specified by the 9 parameters γ, w_0, w_a, Ω_m, σ_8, h, n_s, b_0, and p_0, where b_0 and p_0 are the parameters for the bias model, for which we adopted the scale independent bias model with the form

$$b(z) = 1 + (b_0 - 1)(1 + z)^{p_0}. \qquad (3.1)$$

Here we assumed the target parameters $b_0 = 1.38$ and $p_0 = 1$. For the theoretical modeling of the galaxy power spectrum and the computation of the Fisher matrix, the
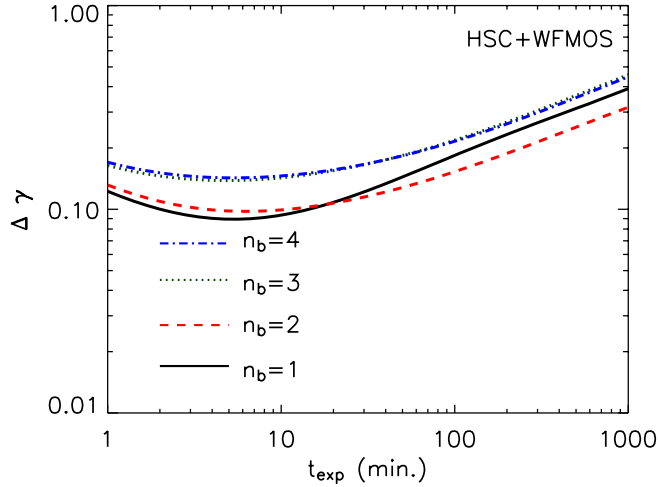
FIG. 7 (color online). Same as Fig. 6, but considering the case of the weak-lensing power spectrum combined with the galaxy power spectrum of the redshift survey.
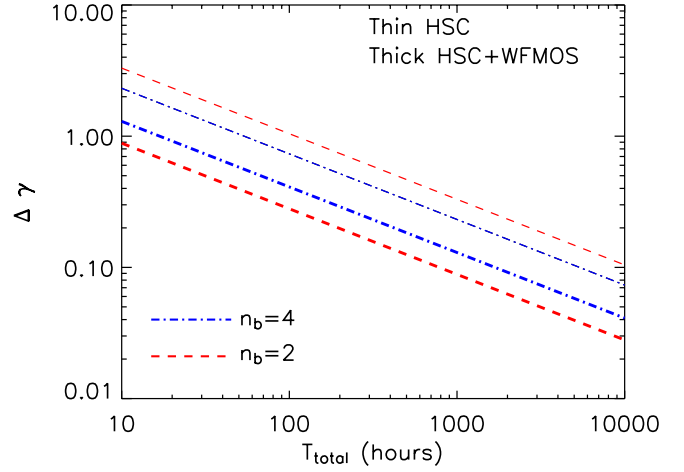

FIG. 8 (color online). 1 sigma error on γ as a function of the total observation time. Here we fixed $t_{exp} = 10$ min and $n_b = 4$(dash-dotted curve) and $n_b = 2$ (dashed curve). The thin curve is the result with the 7 parameters of the Fisher matrix for the lensing power spectrum, but the thick curve is the constraint from the combined weak-lensing power spectrum and galaxy power spectrum (from a redshift survey).

range of the wave number $0.01h\,\mathrm{Mpc}^{-1} \leq k \leq 0.2h\,\mathrm{Mpc}^{-1}$ is included, (see the appendix for details).

From Figs. 6 and 7, the error of γ has a minimum of t_{exp} between several minutes and 100 minutes, depending on the strategy. For the weak-lensing survey (HSC) alone, the tomography technique is very effective in reducing the error, and the result is fairly insensitive to the choice of t_{exp}. An additional spectroscopic survey (WFMOS) significantly reduces the error. In this case, shallow surveys with $t_{exp} < 10$ min provide the minimum error for γ. Especially, the case $n_b = 1$ and $n_b = 2$ is significantly improved by the combination. This behavior is understood as follows. We assume the total observation time of the WFMOS survey is not fixed, while adopting the same survey area as the HSC survey. Then, in these figures, the cases $n_b = 1$ and $n_b = 2$ assume a larger survey area for the redshift survey than that of the cases $n_b = 3$ and $n_b = 4$. However, note that the minimum is located around the several minutes of the exposure time even for the case $n_b = 3$ and 4. Therefore, when considering the combination with the redshift survey, wider and shallower surveys are indeed preferred.

Now we are in a position to answer the question: is it possible to distinguish between the DGP and dark energy models? For that purpose, $\Delta\gamma \lesssim 0.1$ is required. Figure 8 plots the 1 sigma error as a function of the total observation time T_{total}, where we adopt $t_{exp} = 10$ min and $n_b = 4$ (dash-dotted curve) and $n_b = 2$ (dashed curve). The thin curve is the result of the weak-lensing survey alone, while the thick curve is the result combined with the redshift survey. Note that $\Delta\gamma$ is in proportion to $T_{total}^{-1/2}$. Figure 8 suggests that the HSC survey alone may reach $\Delta\gamma < 0.1$ with $T_{tot} = 10^4$ h, the combination with the WFMOS survey may do so with $T_{tot} = 10^3$ h if we put a prior constraint on Ω_b.

Finally in this section, let us consider other impact that the HSC survey may present as a test of modified gravity models. The dash-dotted curves in Fig. 9(a) show the 1, 2, and 3-sigma confidence contours (going from the innermost outward) in the w_0-w_a plane, by marginalizing the Fisher matrix of the 7 parameters, γ, w_0, w_a, Ω_m, σ_8, h, and n_s, over the parameters other than w_0 and w_a. Here the constraint from the future Planck survey is taken into account by including the prior constraints $\Delta\Omega_m = 0.035$, $\Delta\sigma_8 = 0.04$, $\Delta w_0 = 0.32$, $\Delta w_a = 1$, $\Delta n_s = 0.0035$ [32]. Here the target parameters are the same as those of the ΛCDM model in Fig. 4, and we fixed $n_b = 4$ and $t_{exp} = 10$ min . Note that the point of the DGP model $(w_0, w_a) = (-0.78, 0.32)$ is marked, and is almost near the 2 sigma curve. This means that the HSC can distinguish between the DGP model and the ΛCDM model at the 2 sigma level by including the future constraint by the observation of the cosmic microwave background anisotropy. Here, we fixed the total observation time as 800 hours, then the constraint can be improved when the total observation time is longer. The solid curve is the combination with the WFMOS survey, which also shows the significant improvement of the constraint. Similarly, Fig. 9(b) shows the 1, 2, and 3-sigma confidence contours in the w_0-γ plane, by marginalizing the Fisher matrix over the parameters other than w_0 and γ. The point of the DGP model $(w_0, \gamma) = (-0.78, 0.68)$ is marked. With this figure, the constraint is at the 1 sigma level. Then we cannot clearly distinguish between the DGP model and the ΛCDM model with this plot. These features reflect how the shear power spectrum is sensitive to the parameters. This suggests the choice of a projection is important for distinguishing between these models.
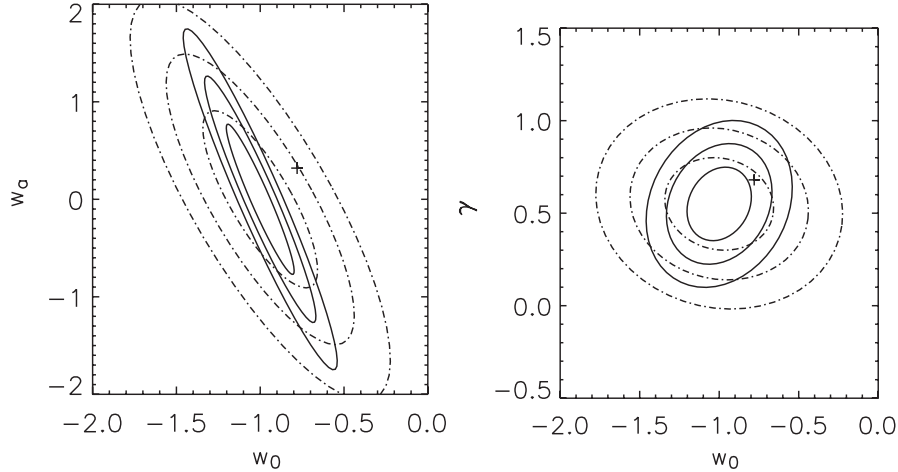
FIG. 9.   (a, left) The 1, 2, and 3-sigma contours in the w_0-w_a plane. The dash-dotted curve is the result with the 7 parameters of the Fisher matrix for the lensing power spectrum and the Planck prior constraint, and the solid curve is these constraints combined with the galaxy power spectrum from a redshift survey. The target model is the ΛCDM model, then $(w_0, w_a) = (-1, 0)$, and the mark $(w_0, w_a) = (-0.78, 0.32)$ is the DGP model. Here we fixed $n_b = 4$, $t_{exp} = 10$ min, and the total observation time, 800 hours. (b, right) Same as (a), but with the contours in the w_0-γ plane from marginalizing the Fisher matrix of the 7 parameters over all other parameters. The target model is the ΛCDM model, then $(w_0, \gamma) = (-1, 0.55)$, and the mark $(w_0, \gamma) = (-0.78, 0.68)$ is the DGP model.

IV. SUMMARY AND CONCLUSIONS

In this paper, we investigated optimization of a weak-lensing survey for the dark energy, and how such a survey might be used for testing modification of the theory of gravity. By introducing a simple model of the survey sample as a function of the exposure time for one band of one field of view, we investigated how the FoM and the constraint on Linder's γ parameter depend on the exposure time and the number of passbands. To optimize the survey to probe modifications of gravity, we considered a figure of merit in the space $\{\gamma, w_0, w_a\}$ as well as in the familiar 2D plane $\{w_0, w_a\}$. We obtained the following results: (1) The peak of the FoM is located at $t_{exp} \simeq$ several ~ 10 min for $n_b = 2, 3, 4$, though the peak profile is very broad. (2) The tomography technique improves the FoM effectively when including the parameter γ. (3) The combination with the redshift survey like the WFMOS BAO survey improves the error on the parameter γ. (4) The shallow and wide survey is advantageous for the tomography, and has potential when taking combination with the redshift survey into account. (5) The HSC weak-lensing survey by itself is not sufficient for distinguishing between the DGP model and a dark energy model with the same background expansion, but it will be able to distinguish between the DGP and ΛCDM at the 2 sigma level by including the prior constraint from future cosmic microwave background (CMB) observation.

We assumed a very simplified model of the survey galaxy sample, and the error in the photometric redshift measurement is not taken into account. Also we assumed that the weak-lensing power spectrum of the $10 \leq l \leq$

$10^4 (N_g/35/n_b)^{1/2}$ can be used. Further investigation is needed including the modeling of the galaxy sample and the error in measuring the photometric redshift. In the present paper, we assumed the spatially flat universe. In general, since the lensing power spectrum is not very sensitive to the curvature of the Universe, then the inclusion of the other parameter will degrade the constraint [33].

APPENDIX A: MODELING OF THE REDSHIFT SURVEY POWER SPECTRUM

Here we briefly review the power spectrum and the Fisher matrix formula for a galaxy redshift survey

[34,35], adopted in the present paper. Here we assume a measurement of the multipole power spectrum $\mathcal{P}_l(k)$ ($l = 0, 2$) from the galaxy redshift survey, which we theoretically model as

$$\mathcal{P}_l(k) = \frac{1}{2} \int d\mu \, \frac{\int d\mathbf{s}\, \bar{n}(\mathbf{s})^2 \psi(\mathbf{s}, k, \mu)^2 P(k, \mu, s) \mathcal{L}_l(\mu)}{\int d\mathbf{s}' \, \bar{n}^2(\mathbf{s}') \psi(\mathbf{s}', k, \mu)^2}, \tag{A1}$$

where $\mathbf{s}$ is the coordinate of the redshift space, $\bar{n}(\mathbf{s})$ is the mean number density per unit volume, $\psi(\mathbf{s}, k, \mu)$ is the weight factor, $\mathcal{L}_l(\mu)$ is the Legendre polynomial, μ is the directional cosine between $\mathbf{k}$ and $\mathbf{s}$, and $P(k, \mu, s[z])$ is the power spectrum at the redshift z, which is modeled as

$$P(k, \mu, s[z]) = \frac{s(z)^2}{\chi(z)^2} \frac{ds(z)}{d\chi(z)} P_{\text{gal}}\Big(q_\parallel \to k\mu \frac{ds(z)}{d\chi(z)}, q_\perp$$
$$\to k\sqrt{1 - \mu^2} \frac{s(z)}{\chi(z)}, z \Big) \tag{A2}$$

with

$$P_{\text{gal}}(q_\parallel, q_\perp, z) = b(z)^2 \bigg[1 + \frac{d\ln D_1(z)/d\ln a(z)}{b(z)} \frac{q_\parallel^2}{q^2} \bigg]^2$$
$$\times P_{\text{mass}}^{\text{Linear}}(q, z), \tag{A3}$$

where $q^2 = q_\parallel^2 + q_\perp^2$, $P_{\text{mass}}^{\text{Linear}}(q, z)$ is the linear mass power spectrum at the redshift z. The comoving distance $\chi[z]$ is given by

$$\chi(z, \Omega_m, w_0, w_a) = \frac{1}{H_0} \int_0^z \frac{dz'}{\sqrt{\Omega_m(1 + z')^3 + (1 - \Omega_m)(1 + z')^{3(1 + w_0 + w_a)} e^{-3w_a z'/(1 + z')}}}, \tag{A4}$$

as is given in Eq. (2.9). For our fiducial model we adopt the flat ΛCDM model with $\Omega_m = 0.27$. Thus, our fiducial model is $s(z) = \chi(z, 0.27, -1, 0)$. In the modeling of the bias, we consider the scale independent bias model in the form, Eq. (3.1).

The variance of $\mathcal{P}_l(k)$ is given by

$$\Delta \mathcal{P}_l(k)^2 = 2 \frac{(2\pi)^3}{\Delta V_k} \mathcal{Q}_l^2(\mathbf{s}, k), \tag{A5}$$

where ΔV_k denotes the volume of the shell in the Fourier space, and we have defined

$$\mathcal{Q}_l^2(k) = \frac{1}{2} \int d\mu \, \frac{\int d\mathbf{s}\, \bar{n}(\mathbf{s})^4 \psi(\mathbf{s}, k, \mu)^4 [P(k, \mu, s) + 1/\bar{n}(\mathbf{s})]^2 [\mathcal{L}_l(\mu)]^2}{[\int d\mathbf{s}' \, \bar{n}(\mathbf{s}')^2 \psi(\mathbf{s}', k, \mu)^2]^2}. \tag{A6}$$

Then, we may evaluate the Fisher matrix by

$$F_{\alpha\beta} \simeq \sum_{l=0,2} \frac{1}{4\pi^2} \int_{k_{\min}}^{k_{\max}} [\mathcal{Q}_l^2(k)]^{-1} \frac{\partial \mathcal{P}_l(k)}{\partial \theta^\alpha} \frac{\partial \mathcal{P}_l(k)}{\partial \theta^\beta} k^2 dk. \tag{A7}$$

In the present paper, we adopt $\bar{n}(s[z]) = 4 \times 10^{-4} h^3 \text{ Mpc}^{-3}$ and $\psi(\mathbf{s}, k, \mu) = 1$.

[1] G. Dvali, G. Gabadadze, and M. Porrati, Phys. Lett. B **485**, 208 (2000).
[2] G. Gabadadze, Astrophys. J. **597**, 566 (2003).
[3] K. Yamamoto, B. A. Bassett, R. C. Nichol, Y. Suto, and K. Yahata, Phys. Rev. D **74**, 063525 (2006).
[4] A. F. Heavens, T. D. Kitching, and L. Verde, arXiv:astro-ph/0703191.
[5] M. Kunz and D. Sapone, Phys. Rev. Lett. **98**, 121301 (2007).
[6] M. A. Luty, M. Porrati, and R. Rattazzi, J. High Energy Phys. 09 (2003) 029.
[7] A. Nicolis and R. Rattazzi, J. High Energy Phys. 06 (2004) 059.
[8] K. Koyama, Phys. Rev. D **72**, 123511 (2005).
[9] R. Maartens and E. Majerotto, Phys. Rev. D **74**, 023004

(2006).
[10] Y.-S. Song, I. Sawicki, and W. Hu, Phys. Rev. D **75**, 064003 (2007).
[11] K. Koyama and R. Maartens, J. Cosmol. Astropart. Phys. 01 (2006) 016.
[12] A. Albrecht *et al.*, arXiv:astro-ph/0609591.
[13] J. A. Peacock *et al.*, arXiv:astro-ph/0610906.
[14] A. Amara and A. Refegier, arXiv:astro-ph/0610127.
[15] D. Parkinson, C. Blake, M. Kunz, B. A. Bassett, R. C. Nichol, and K. Glazebrook, Mon. Not. R. Astron. Soc. **377**, 185 (2007).
[16] M. Chevallier and D. Polarski, Int. J. Mod. Phys. D **10**, 213 (2001).
[17] E. V. Linder, Phys. Rev. Lett. **90**, 091301 (2003).
[18] R. Crittenden, E. Majerotto, and F. Piazza, arXiv:astro-ph/

0702003 [Phys. Rev. Lett. (to be published)].

[19] E. V. Linder, Phys. Rev. D **72**, 043529 (2005).

[20] D. Huterer and E. V. Linder, Phys. Rev. D **75**, 023519 (2007).

[21] E. V. Linder and R. N. Cahn, arXiv:astro-ph/0701317.

[22] M. Takada and M. White, Astrophys. J. **601**, L1 (2004).

[23] W. Hu, Astrophys. J. **522**, L21 (1999).

[24] D. Huterer, M. Takada, G. Bernstein, and B. Jain, Mon. Not. R. Astron. Soc. **366**, 101 (2006).

[25] D. Dolney, B. Jain, and M. Takada, Mon. Not. R. Astron. Soc. **366**, 884 (2006).

[26] J. A. Peacock and S. J. Dodds, Mon. Not. R. Astron. Soc. **280**, L19 (1996).

[27] O. Ilbert *et al.*, Astron. Astrophys. **457**, 841 (2006).

[28] S. Miyazaki *et al.*, Publ. Astron. Soc. Jpn. **54**, 833 (2002).

[29] B. Jain, A. Connolly, and M. Takada, J. Cosmol. Astropart. Phys. 03 (2007) 013.

[30] K. Koyama and F. P. Silva, Phys. Rev. D **75**, 084040 (2007).

[31] M. Ishak, A. Upadhye, and D. N. Spergel, Phys. Rev. D **74**, 043513 (2006).

[32] S. Wang, J. Khoury, Z. Haiman, and M. May, Phys. Rev. D **70**, 123008 (2004).

[33] C. Clarkson, M. Cortes, and B. A. Bassett, arXiv:astro-ph/0702670.

[34] K. Yamamoto, M. Nakamichi, A. Kamino, B. A. Bassett, and H. Nishioka, Publ. Astron. Soc. Jpn. **58**, 93 (2006).

[35] K. Yamamoto, B. A. Bassett, and H. Nishioka, Phys. Rev. Lett. **94**, 051301 (2005).